Dichloroacetate reverses sepsis-induced hepatic metabolic dysfunction

Rabina Mainali[1*], Manal Zabalawi[2*], David Long[2], Nancy Buechler[1], Ellen Quillen[2], Chia-Chi Key[2], Xuewei Zhu[2], John Parks[2], Cristina Furdui[2], Peter W. Stacpoole[3], Jennifer Martinez[4], Charles E. McCall[2#], Matthew A, Quinn[1,2,5#]

[1]Department of Pathology, Section on Comparative Medicine Wake Forest School of Medicine, Winston-Salem, North Carolina

[2]Department of Internal Medicine, Section of Molecular Medicine Wake Forest School of Medicine, Winston-Salem, North Carolina

[3]Division of Endocrinology, Diabetes and Metabolism and Department of Biochemistry and Molecular Biology, University of Florida College of Medicine, Gainesville, Florida

[4]Immunity, Inflammation, and Disease Laboratory, National Institute of Environmental Health Sciences (NIEHS), National Institutes of Health (NIH), Research Triangle Park, NC

[5]Lead Contact

* these authors contributed equally
# denotes co-corresponding author

Corresponding Authors:

Matthew A. Quinn, Ph.D.
Wake Forest School of Medicine
Medical Center Blvd
Winston-Salem, NC 27157
Office: 336-713-1995
mquinn@wakehealth.edu

Charles E. McCall, M.D.
Wake Forest School of Medicine
Medical Center Blvd
Winston-Salem, NC 27157
Office: 336 413 8034
chmccall@wakehealth.edu

Keywords: sepsis, mitochondria function, liver, inflammation, metabolism, steatosis

Abstract

Dramatic metabolic reprogramming between an anabolic resistance and catabolic tolerance state occurs within the immune system in response to systemic infection with the sepsis syndrome. While metabolic tissues such as the liver are subject to end-organ damage during sepsis and are the primary cause of sepsis death, how their metabolic and energy reprogramming during sepsis state ensures survival is unclear. Employing comprehensive metabolomic screening, targeted lipidomic screening, and transcriptional profiling in a mouse model of septic shock, we show that hepatocyte lipid metabolism, mitochondrial TCA energetics, and redox balance are significantly reprogramed after cecal ligation and puncture (CLP). We identify increases in TCA cycle metabolites citrate, cis-aconitate, and itaconate with reduced fumarate, elevated triglyceride synthesis, and lipid droplet accumulation in the septic hepatocytes. Transcription analysis of liver tissue supports and extends the hepatocyte findings. Strikingly, the administration of the pyruvate dehydrogenase kinase (PDK) inhibitor dichloroacetate (DCA) reverses dysregulated hepatocyte metabolism and mitochondrial dysfunction. Our data indicate sepsis promotes hepatic metabolic dysfunction. Furthermore, our data indicate that targeting the mitochondrial PDC/PDK energy homeostat rebalances transcriptional and metabolic manifestations of sepsis within the liver.

Sepsis is a potentially life-threatening condition that occurs due to the body's overwhelming response to an infection. This reaction leads to aberrant immune responses and if not diagnosed and treated early after its onset, may limit survival by inducing coagulopathy, altered microvasculature, and dysregulation of the host's metabolism and organ function [1-7]. Sepsis accounts for one in three hospital deaths in the U.S. and millions of deaths each year globally, highlighting its hazard to public health [8,9]. The high mortality rate associated with sepsis reflects the lack of a clinically viable molecular-based therapeutic target. Therefore, understanding the pathogenesis of sepsis at both the molecular and organismal level is of utmost importance to address major gaps in knowledge regarding sepsis.

The response to sepsis has classically been characterized as a biphasic phenomenon, where the acute phase is characterized by high energy consumption and hyper-inflammation associated with oxidative stress, followed by cellular reprogramming to a low energy, anti-inflammatory state of immunometabolic paralysis, with accompanying organ failure [8,10-12]. Additionally, during the early phase of sepsis increased catabolism of fats, proteins, and carbohydrates, associated with high rates of oxygen consumption and ATP synthesis is observed [13-16]. Following the acute phase is a hypometabolic state where ATP production and mitochondrial respiration decreases [13]. It is postulated that this is a protective mechanism to overall lower the metabolic demands of the cell and help with its recovery [1,17,18].

Of particular interest to us, during the hyper-inflammatory anabolic phase of sepsis, an increase in the expression and activity of pyruvate dehydrogenase kinase 1 (PDK1) consistently occurs [19,20]. This enzyme is one of four PDK isoforms that reversibly phosphorylates serine residues on pyruvate dehydrogenase complex (PDC) E1a subunit, inhibiting the conversion of pyruvate to acetyl coenzyme A (acetyl CoA) [21]. Inhibition of this important enzymatic activity that connects glycolysis to tricarboxylic acid (TCA) cycle, oxidative phosphorylation (OXPHOS), and the lipogenic pathway is thought to be an important mechanism driving the dysfunction of mitochondrial respiration and cell bioenergetics observed during sepsis [19,22]. Therefore, PDK serves as a potential therapeutic target as it can allow for the downstream oxidation of glucose to continue, restoring

OXPHOS and mitochondrial functioning that we know to be altered in both immune and non-immune cells during sepsis [16,19,23,24].

The liver is an important metabolic and immune organ due to its role in nutrient metabolism and production of acute phase proteins. However, our understanding of transcriptional alterations and subsequent metabolic manifestations elicited by sepsis still remain limited [16,25-28]. Furthermore, the effects of DCA at restoring hepatic metabolic function in the context of sepsis is completely unknown. Hence, we set out to characterize the global hepatic manifestations of sepsis, with the overall goal of identifying global metabolic pathways subject to dysregulation and whether these pathways are under regulation of DCA.

Results

Sepsis Impairs Hepatic Mitochondrial Metabolism

To test the long-term hepatic transcriptional changes elicited by sepsis we performed RNA-seq in whole livers thirty-hours post cecal ligation puncture (CLP). At this time point, septic mice exhibit tolerance, in which immunometaboic paralysis and end organ dysfunctions decrease survival. Ingenuity pathway analysis (IPA) of the top physiological pathways subject to alteration in response to sepsis revealed a significant increase in the acute phase response pathway, highlighting a persistent inflammatory state in the liver into the chronic phase of sepsis (Fig. 1a). Of particular interest were the findings that oxidative phosphorylation and mitochondrial dysfunction were the top two enriched pathways in the liver of septic mice (Fig. 1a). To gain further insight into the effects of sepsis on the transcriptional regulation of mitochondrial function we performed gene set enrichment analysis (GSEA) of the oxidative phosphorylation pathway (GO:0006119). Septic mice at 30 h decreased the transcriptional output of OXPHOS components, as evidenced by a negative GSEA enrichment score (Fig. 1b). Given the connection between oxidative phosphorylation and the tricarboxylic acid (TCA) cycle, we next asked if polymicrobial infection would elicit similar alterations in this pathway. In accordance with the changes observed in the oxidative phosphorylation pathway, we found a negative enrichment score for TCA cycle enzymes (GO:0006099) in the liver of CLP mice (Fig. 1c). Thus, our transcriptome data indicate that sepsis impairs mitochondrial metabolism in the liver.

Next we wanted to assess if the transcriptional changes elicited by sepsis would manifest in altered hepatic TCA cycle metabolism. Therefore, we performed global

149 unbiased metabolomic screening in isolated hepatocytes from control and septic mice by
150 Ultrahigh Performance Liquid Chromotography-Tandem Mass Spectroscopy (UPLC-
151 MS/MS). In line with altered transcriptional regulation of the TCA cycle, we found that
152 sepsis altered the relative abundance of multiple metabolites involved in the TCA cycle
153 (Fig. 1d). In particular, significant elevation of citrate and cis-aconitate was observed in
154 septic hepatocytes at 30h (Fig. 1e&f). Unlike macrophages, which shift their ratio of
155 succinate and α-ketoglutarate to favor succinate accumulation over α-ketoglutarate [29-31],
156 we found no changes in the levels of these metabolites in hepatocytes (Fig. 1G&H).
157 Furthermore, unlike macrophages [32], levels of fumarate decreased, but malate levels
158 were unchanged in hepatocytes from septic animals (Fig. 1I&J). Monocytes,
159 macrophages and dendritic cells reprogram the TCA cycle during acute inflammation to
160 a catabolic tolerance phenotype by shunting cis-aconitate to itaconate through the
161 enzymatic action of aconitase decarboxylase (ACOD1; also known as immune
162 responsive gene 1 [IRG1]) [32-35]. Accordingly, we also found that sepsis significantly
163 induces *ACOD1* and elevates itaconate in isolate hepatocyte preparations (Fig. 1K&L).
164

165 **Sepsis Impairs Hepatic Redox Balance and Promotes Oxidative Stress**

166 Perturbations in oxidative phosphorylation have been shown to promote the
167 production of reactive oxygen species (ROS) [36]. Furthermore, itaconate has been shown
168 to induce genes involved in oxidative stress regulation through activation of the master
169 NRF2 KEAP1 antioxidative pathway in macrophages [34]. Therefore, we examined if sepsis
170 invokes a gene expression profile involved in regulation of ROS. GSEA of the ROS
171 metabolic process pathway (GO:0072593) revealed a positive enrichment, highlighting

172 the transcriptional induction of genes involved in the regulation of oxidative stress in livers
173 of septic mice (Fig. 2a). Given the induction of ROS metabolic genes we wanted to
174 determine if sepsis alters key metabolites involved in redox balance, specifically the
175 cysteine-glutathione transsulfuration redox regulatory cycle. Sepsis did not alter
176 intracellular homocysteine levels in islated hepatocytes (Supplemental Fig. 1), however,
177 cystathionine decreased significantly (Fig. 2b). Furthermore, we found a trend for
178 decreased cysteine levels in the liver (p=0.0534) (Fig. 2c) and significantly decreased
179 glycine (Fig. 2d). Most dramatically, septic mice depleted hepatocyte glutathione (Fig. 2e)
180 and led to decreases in oxidized glutathione (GSSG) (Fig. 2f). Ophthalamate has recently
181 been shown to be a biomarker of oxidative stress and signals consumption of hepatic
182 GSH [37]. Functionally we observe a significant accumulation of hepatic ophthalamate
183 levels in response to sepsis, signifying a state of oxidative injury (Fig. 2g).
184

185 **Sepsis promotes hepatic steatosis**

186 Thus far, our data has revealed that sepsis induces significant impairments in
187 hepatocyte OXPHOS, alterations in the TCA cycle, and induction of oxidative stress, find-
188 ings that are also metabolic hallmarks of fatty liver disease [38]. Because perturbations in
189 global lipid profiles occur in septic patients [15], we evaluated the effects of CLP on the
190 hepatic lipid metabolism pathway. In support of our hypothesis that sepsis alters hepatic
191 lipid metabolism, transcriptome data indicate significant repression of lipid metabolism in
192 livers of septic mice (Fig. 3a). Sepsis also decreased transcription output that supports
193 fatty acid metabolic process components in the liver, as evidenced by a negative GSEA

194 enrichment score (Fig. 3b). In particular, we find alterations in genes involved in both fatty
195 acid oxidation as well as fatty acid biosynthesis (Supplemental Fig. 2).

196 Since transcriptional regulation of hepatic lipid metabolism is significantly altered
197 during sepsis, we further investigated the functional manifestation of these gene expres-
198 sion profile. Consistent with our transcriptional profiling studies, our unbiased metabo-
199 lomic screening in hepatocytes also identified lipid metabolism as the top metabolic path-
200 way altered in sepsis (Fig.3c). We observe increases in virtually all fatty acids and acyl-
201 carnitine derivatives assayed (Fig. 3d). The dysregulation in hepatic lipid metabolism in
202 response to sepsis ultimately culminates in the development of steatosis, as evidenced
203 by increased free fatty acids, mono-, di- and triglycerides (Fig. 3e).

204

205 **Sepsis remodels the hepatic lipidome**

206 Given the severe dysregulation in hepatic lipid metabolism triggered by sepsis, we
207 next sought to characterize the global consequences on hepatic lipid profiles. This was
208 achieved by targeted lipidomic screening. Parallel to our unbiased metabolomic
209 screening, we find sepsis leads to profound accumulation of almost all lipid species
210 surveyed (Fig. 4a). We next evaluated the hepatic lipid composition to discern which lipid
211 species are must vulnerable to sepsis-induced alterations. We find very little alterations
212 to the ceramide pool in septic hepatocytes (Fig. 4b) with only modest changes in
213 dihydroceramide (Supplemental Fig. that the fatty acid and phospholipid fraction are most
214 sensitive to alterations in response to sepsis (Fig. 4b). However, the hepatic fatty acid
215 fractions displayed significant remodelling in response to sepsis (Fig. 4b). Morever,
216 hepatic phospholipid composition showed robust alterations following CLP (Fig. 4b). Of

217 the phospholipids (PLs) most significantly affected, we find accumulation of
218 phosphotidylcholines (PCs), phosphotidylethanolamine (PE) and sphingomyelin (SM)
219 (Fig. 4c). Of the hepatic PC pool we find the most abundant species (16:0/18:2 &
220 16:0/18:1) to show increased accumulion in response to sepsis (Supplemental Fig. 4a).
221 We also observed significant increases in the most abundant PE species (18:0/20:4,
222 16:0/22:6 & 18:0/22:6) and SM species (22:0, 16:0 & 20:0) to show significant
223 accumulation in septic hepatocytes (Supplemental Fig. 4b&c). We did observe a
224 decrease in one phospholipid species, lysophosphatidylcholine, however, the hepatic
225 concentration of this phospholipid species is signifcantly lower than other PL species
226 assayed (Fig. 4c). Finally, we detected no differences in other PL species such as
227 phosphotidylinositol (PI) and lysophosphatidylethanolamine (LPE) and no differences in
228 hepatic cholesterol ester levels (Supplemental Fig. 5). Our data collectively detail the
229 impact of sepsis on hepatic lipid composition and robustly show a global rise in nearly all
230 lipid species.
231

232 **PDK inhibition attenuates sepsis-induced transcriptional and metabolic changes**
233 **in the liver**

234 We have previously reported that PDK inhibition by the pyruvate analog and pan-
235 PDK inhibitor dichloroacetate (DCA) promotes PDC-dependent immunometabolic adap-
236 tations to sepsis and increases survival [19,39]. Given the establishment of hepatocyte mi-
237 tochondrial dysfunction and steatosis during sepsis, we asked whether pharmacological
238 targeting of the hepatic PDK/PDC axis would mitigate the disruption of key metabolic and
239 bioenergetic processes induced by sepsis. To test this postulate, we administered DCA

240 to septic mice 24 h after CLP onset and assessed the global transcription profile of liver
241 6 h later via RNA-seq. DCA treatment of septic mice reversed the majority of sepsis-
242 regulated gene networks (Fig. 5a). Most notably, pathways involved in redox homeosta-
243 sis, lipid metabolism and mitochondrial dysfunction are returned to control levels with the
244 administration of DCA in septic mice (Fig. 5b).

245 Given our previous results indicating the transcriptional changes associated with
246 sepsis in the liver underlie functional alterations in metabolism, we wanted to determine
247 if the DCA reversal of transcriptional changes mounts to differential metabolomes. Given
248 our RNA-seq data showing a positive enrichment score for production of ROS along with
249 negative enrichment for glutathione conjugation, we started off with evaluating the redox
250 pathway metabolites. Strikingly, the depletion of redox components cystathionine, cyste-
251 ine, glycine, hypotaurine, taurine and glutathione elicited by sepsis was completely re-
252 versed by administration of DCA (Fig. 5c). More importantly, we observed a significant
253 decrease in hepatic ophthalmate levels, signifying a functional decrease in oxidative
254 stress (Fig. 5c). The restoration in redox metabolites in septic mice following DCA admin-
255 istration prompted us to investigate the mitochondrial consequences of this pharmaco-
256 logical intervention. With the exception of fumarate, DCA completely restores TCA me-
257 tabolite levels to that of sham levels (Fig. 5d). Finally, we wished to define the effects of
258 DCA treatment on the hepatic lipidome. Lipidomic analysis shows a protective effect of
259 DCA in ameliorating sepsis-induced steatosis. In sum, these data reveal pharmacological
260 inhibition of the PDK pathway restores transcriptional and metabolic changes associated
261 with sepsis in the liver.

262

Discussion

Considerable attention has been focused recently on the immunometabolic consequences of inmflammation in immune cells [40]. However, significant gaps exist in our understanding of the metabolic adaptations induced by systeminc inflammation from sepsis in vital organs. Addressing this limitation is critical because sepsis survival depends on restoring both organ and immune cell homeostasis following dysregulated and disseminated inflammation [41]. In the present study we reveal severe disruption of several key hepatic metabolic pathways in septic mice, including TCA cycle activity, OXPHOS, redox balance and lipid metabolism. Importantly, DCA administration restored TCA cycle flux, restored rerdox balance and ameliorated sepsis-induced steatosis. Our study highlights the clinical potential of targeting the PDC/PDK axis in restoring liver function/metabolism in the context of sepsis.

Remodelling of TCA cycle flux is well appreciated to support immune cell effector function in the face of inflammatory challenges [3,31,42,43]. For example, succinate primes inflammation through succinate dehydrogenase (SDH)-mediated ROS generation and ATP synthesis [31,42]. SDH-derived ROS enhances IL-1β production by activating HIF-1α and activating the NLRP3 inflammasome [20]. Inhibition of SDH activity increases IL-10 production and skews inflamed immune cells towards an anti-inflammatory response [31]. Fumarate, on the other hand, possesses anti-inflammatory properties as it inhibits pro-inflammatory cytokine production either by activating the NRF2 pathway or via inhibiting pathways like NF-κB and MAPK that lie downstream of TLR signaling in immune cells [44,45]. Our findings extend the concept that the TCA cycle is subject to reprogramming in response to sepsis in non-immune cells such as hepatocytes. Furthermore, we found

286 similarities as well as differences in terms of TCA cycle remodelling in hepatocytes com-
287 pared to immune cell effects, clearly indicating this pathway is regulated in a cell-type and
288 context-dependent manner during sepsis.

289 In response to LPS stimulation, macrophages significantly upregulate IRG1 and
290 accumulate itaconate from the decarboxylation of cis-aconitate [32,34]. One of the primary
291 functions itaconate serves in immune cells is to limit IL-1 β production through direct
292 inhibition of SDH and activation of the NRF2/Keap1 and IκBζ-ATF3 pathways [32,34,46]. In
293 line with what occurs in macrophages, we observed an increase in IRG1 and itaconate in
294 septic hepatocytes at 30h. While we did not fully characterize the hepatic function of
295 itaconate, a recent paper demonstrates its anti-inflammatory effects during Ischemia-
296 reperfusion (IR) injury in the liver [47]. The deletion of IRG1 heightens inflammation and
297 liver damage and renders hepatocytes susceptible to oxidative injury after I/R injury.
298 Further, itaconate administration reduces liver damage and inflammation associated with
299 I/R in IRG1 KO mice, also emphasizing its anti-inflammatory and hepatoprotective effects
300 [47]. Given the immunomodulatory effects of itaconate and its accumulation in the liver in
301 our study, we hypothesize that itaconate directs hepatocyte shifts in both TCA cycle
302 metabolism and mitochondrial energetics. DCA reduces itaconate levels, which we also
303 find in a human monocyte model of sepsis [48].

304 Similar to immune cells, liver cells increase ROS production during sepsis [49,50].
305 We offer a potential mechanism whereby sepsis leads to significant depletion of redox
306 metabolites within the glutathione pathway ultimately culminating in loss of cellular
307 glutathione levels resulting in ophthalamate accumulation in hepatocytes.

308 Sepsis profoundly alters lipid metabolism, resulting in significant increases in
309 plasma fatty acid and glycerol concentrations, changes reported to predict prognosis in
310 septic patients [51]. Furthermore, patients who died from sepsis had evidence of hepatic
311 steatosis affecting 5%-80% of liver parenchyma [52]. Human data supports a robust hepatic
312 steatosis phenotype subsequent to sepsis. One vital lipid metabolic pathway which can
313 contribute to steatosis is *de novo* lipogenesis. While we did not directly measure hepatic
314 lipogenesis, our metabolomics screening did show an increase in hepatic citrate and free
315 fatty acid levels suggesting an increased lipogenic drive during sepsis. Functionally,
316 immune cells exploit the lipogenic pathway for the generation of malonyl-CoA and
317 subsequent malonylation of glycolytic enzymes, which ultimately contributes to the
318 metabolic adaptation of macrophages to inflammatory cues [53]. Future studies dissecting
319 the role of lipogenesis in altering hepatocyte function during systemic infection are
320 warranted.

321 In addition to accumulation of free fatty acids and triglycerides in the liver, our
322 lipidomic analysis revealed significant increases in phospholipids. In the present study,
323 we find hepatic levels of the phospholipids phosphatidylcholine,
324 phosphatidylethanolamine, and sphingomyelin to be heightened during sepsis, indicating
325 abnormal metabolism of phospholipids. PC and PE are the most abundant phospholipids
326 that make up cellular membranes and an abnormally high ratio of PC and PE has been
327 reported to influence energy metabolsm and linked to fatty liver disease and impairement
328 in liver regeneration after injury [54-56]. Altered PC: PE ratio has also been shown to
329 influence the dynamics and regulation of lipid droplets contributing towards steatosis, a
330 phenotype we also report in our study [54,55,57]. The dysregulation of hepatic phospholipid

331 metabolism may be a contributing mechanism underlying steatosis which is a topic of
332 future investigation. Additionally, phospholipids serve as precursor molecules to bioactive
333 lipids which are involved in numerous signal transduction cascades [58]. Investigating
334 whether signaling properties of bioactive lipids in the liver during sepsis is pathogenic or
335 contributes to sepsis resolution is also needed in the future.

336 PDC is a master metabolic regulator controlling the conversion of pyruvate to
337 acetyl-CoA in the mitochondria [59] . A part of the metabolic reprogramming that occurs in
338 immune cells in response to inflammatory signaling is inactivation of PDC [22,59]. PDK is a
339 negative regulator of the PDC, as it phosphorylates PDC and inhibits the conversion of
340 pyruvate to acetyl-CoA [59]. During sepsis, the expression and activity of PDK1 in immune
341 cells is heightened, contributing to the dysfunction of mitochondria metabolism. One
342 mechanism driving this observed increase is through pro-inflammatory mediators such as
343 LPS and interferon gamma (IFN-γ) [60]. Another possible mechanism contributing to PDK
344 activation in the context of sepsis is through glucocorticoid signaling [61]. In fact, starvation
345 is well established to activate the PDK pathway [62-66]. Based on our findings of elevated
346 glucocorticoid levels in both the circulation and the liver, we hypothesize the stress
347 hormone pathway as a contributor to PDK activation during sepsis.

348 We reported in a sepsis monocyte model that DCA reduced TCA cycle catabolic
349 effects concurrent with increasing amino acid anaplerotic catabolism of branched-chain
350 amino acids, leading to increased TCA-driven anabolic energetics [22]. In the present
351 study, we find restoration of hepatic TCA metabolites, decreased triglyceride
352 accumulation, lessening of lipid synthesis and oxidative stress rebalances in septic mice

after DCA administration. Overall we demonstrate that hepatic transcriptional and metabolic dysfunction improves after targeting the PDC/PDK axis with DCA.

Further work elucidating the mechanistic pathways involved in the dysfunction of lipid metabolism and the impact of TCA metabolite alterations is warranted. In particular, further investigation specifically into the PDK pathway to determine which isoform underlies the hepatic manifestions of sepsis. This is warranted given multiple isoforms of PDK expressed in the liver [67] and DCA inhibits multiple isoforms of PDK [68,69]. The results of this study fill a gap in understanding how sepsis at the molecular level compromises liver function. It also further informs the novel therapeutic targeting potential of the PDC/PDK homeostat.

375

376

377 **Material and Methods**

378

379

380 **Animal Experiments**

381 Male C57BL/6J mice aged 8-10 weeks were purchased from The Jackson Laboratory
382 (Bar Harbor, ME). All animals were subject to a 12:12 hour dark/light cycle with *ad libitum*
383 access to standard rodent chow and water. Cecal ligation puncture model was used to
384 induce sepsis as previously described [39,70]. Briefly, cecum was ligated and punctured two
385 times with a 22-gauge needle. Contents were then returned and incision was closed in
386 two layers (peritoneum and skin). Sham operation where abdominal incision was made
387 but cecum not ligated or punctured was used as a control. Subcutaneous fluids (1ml
388 normal saline) were given to each animal. Mice were euthanized 30 hours post-surgery
389 for tissue collection. Dichloroacetate (DCA) (Sigma; MO, USA) was administered
390 (25mg/kg) intraperitoneally at various time points post-surgery: for metabolomic
391 screening and RNA-seq DCA was administered 24 hours post-surgery and tissues
392 collected 6 hours post DCA administration (30 hours post-surgery), for metabolic cages
393 DCA was administered immediately post-surgery.

394

395 **Hepatocyte Isolation**

396 Hepatocytes were isolated via portal vein perfusion and collagenase digestion as
397 previously described [71]. Following perfusion, liver cells were liberated by gentle
398 dissocation in DMEM (ThermoFisher; CA, USA). Cells were then filtered through nylon
399 mesh to remove cellular debris and connective tissue and resulting cells pelleted by

400 centrifugation at 50g for 1 minute. After three washes with DMEM cells were counted and
401 viability assessed via Trypan Blue exclusion.
402
403 **RNA-sequencing**
404 RNA was isolated from whole liver tissues using Trizol and the RNeasy RNA isolation kit
405 (Qiagen; MD, USA) according to manufacturer's protocol. One microgram of high quality
406 RNA (RIN>8) was used as a template for library generation using the Illumina TruSeq
407 RNA Sample Prep Kit v2 (Illumina; CA, USA) according to the manufacturer's protocol.
408 Generated libraries were then poly(A) enriched for mRNA prior to sequencing. Indexed
409 samples were sequenced at 100bp-paired-end protocol with the NovaSeq 6000
410 (Illumina), generating approximately 20-30 million reads per sample. Sequenced reads
411 were aligned to the University of California Santa Cruz (UCSC) mm10 reference genome
412 using STAR v2.5 as previously described [72]. The mapped read counts were quantified by
413 Subread feature Counts v1.5.0-p1 [73]. Differentially expressed genes (DEGs) were
414 determined by DESeq2 v1.14.1 [73] using a false discory rate of 0.05. Ingenuity Pathway
415 Analysis (Qiagen) and Gene Set Enrichment Analysis v4.0.3 (GSEA) were further used
416 as previously described [74].
417
418 **Ultrahigh Performance Liquid Chromatography-Tandem Mass Spectroscopy**
419 Hepatocytes were isolated described above for metabolomic screening via Ultrahigh
420 Performance Liquid Chromotography-Tandem Mass Spectroscopy (UPLC-MS/MS)
421 (Metabolon; NC, USA). Briefly, 150-200 microliter cell pellets per animal were used as
422 starting material. Samples were prepared using the automated MicroLab STAR system

423 (Hamilton; NV, USA). Proteins were precipitated using methanol under vigorous shaking
424 for 2 minutes followed by centrifugation. Prior to analysis organic solvents were removed
425 with TurboVap (Zymark; MA, USA) and overnight storage under nitrogen. Dried samples
426 were reconstituted with solvents compatible with the three following analytical methods:
427 1) reverse phase (RP)/UPLC-MS/MS methods with positive ion mode electrospray
428 ionization (ESI), 2) RP/UPLC-MS/MS with negative ion mode ESI and 3) HILIC/UPLC-
429 MS/MS with negative ion mode ESI. Resulting samples were analyzed with the ACQUITY
430 UPLC (Waters; MA, USA) and a Q-Exactive high resolution/accurate mass spectrometer
431 (ThermoScientific; MA, USA) interfaced with a heated electrospray ionization (HESI-II)
432 source and Orbitrap mass analyzer operated at 35,000 mass resolution. An acidic positive
433 ion condition was used on an aliquot optimized to detect more hydrophilic compounds.
434 Another acidic positive ion condition was ran but chromotographically optimized for
435 hydrophobic compounds. Basic negative ion optimized conditions was also used on a
436 separate C18 column. Resulting raw data was extracted and peaks identified using
437 Metabolon's hardware and software. Compounds were identified by comnparing to known
438 library entries of purified standards or recurrent unknown entities. A lirary of authenticated
439 standards containing retention time/index (RI), mass to charge ratio (*m/z*) and
440 chromotographic data (MS/MS spectral data) on all library compounds. Three criteria are
441 used to identify chemicals: 1) RI within a narrow window of proposed identification, 2)
442 accurate mass match to the library ± 10 ppm and 3) MS/MS forward and reverse scores
443 between the experimental data and authentic standards. Peaks were quantified using
444 area under the curve (AUC). For complex lipid panel lipids were extracted with
445 methanol:dichloromethane in the presence of internal standards. Extracts were

446 concentrated under nitrogen and reconstituted in 250ml of 10mM ammonium acetate
447 dichloromethane:methanol (50:50). Mass spec analysis was performed in a Shimazdu LC
448 with nano PEEK tubing and the Sciex SlexIon-5500 QTRAP (Sciex; MA, USA). Both
449 negative and positive mode electrospray was used. Individual lipid species were
450 quantified by taking the peak area ratios of target compounds and their assigned internal
451 standards then multiplying by the concentration of added internal standards. Lipid class
452 concentrations were calculated from the sum of all molecular species within a class, and
453 fatty acid compositions were determined by calculating the proportion of each class
454 comprised by individual fatty acids.

455

456
457
458
459
460
461
462

463
464
465
466
467
468

469 **Acknowledgements**

470

471 The authors of this manuscript would like to thank the National Institute of Environmental
472 Health Sciences Epigenomics and DNA Sequencing Core for their help with RNA-
473 sequencing and Dr. Sara Grimm for her analysis of transcriptome data. This work was
474 supported by NIH Intramural Program 1ZIAES10328601 (J.M.), NIH R01 HL132035
475 (X.Z.), NIH K01 DK117069 (C.K), NIH K01 AG056663 (E.Q.), NIH R01 AI065791
476 (C.E.M.), R01 GM102497 (C.E.M.), R35 GM126922 (C.E.M.).

Citations

1 Lewis, A. J., Billiar, T. R. & Rosengart, M. R. Biology and metabolism of sepsis: innate immunity, bioenergetics, and autophagy. *Surgical infections* **17**, 286-293 (2016).

2 Bermudes, A. C. G. *et al.* Changes in lipid metabolism in pediatric patients with severe sepsis and septic shock. *Nutrition* **47**, 104-109 (2018).

3 Cheng, S.-C. *et al.* Broad defects in the energy metabolism of leukocytes underlie immunoparalysis in sepsis. *Nature immunology* **17**, 406 (2016).

4 Levi, M. & van der Poll, T. Coagulation and sepsis. *Thrombosis research* **149**, 38-44 (2017).

5 Schneck, E. *et al.* Plasma DNA and RNA differentially impact coagulation during abdominal sepsis—an explorative study. *Journal of Surgical Research* **210**, 231-243 (2017).

6 McDonald, B. *et al.* Platelets and neutrophil extracellular traps collaborate to promote intravascular coagulation during sepsis in mice. *Blood, The Journal of the American Society of Hematology* **129**, 1357-1367 (2017).

7 Kidokoro, A., Iba, T., Fukunaga, M. & Yagi, Y. Alterations in coagulation and fibrinolysis during sepsis. *Shock (Augusta, Ga.)* **5**, 223-228 (1996).

8 Rhee, C. *et al.* Incidence and trends of sepsis in US hospitals using clinical vs claims data, 2009-2014. *Jama* **318**, 1241-1249 (2017).

9 Buchman, T. G. *et al.* Sepsis Among Medicare Beneficiaries: 1. The Burdens of Sepsis, 2012–2018. *Critical Care Medicine* **48**, 276 (2020).

10 Osuchowski, M. F., Craciun, F., Weixelbaumer, K. M., Duffy, E. R. & Remick, D. G. Sepsis chronically in MARS: systemic cytokine responses are always mixed regardless of the outcome, magnitude, or phase of sepsis. *The Journal of Immunology* **189**, 4648-4656 (2012).

11 Chiswick, E. L., Mella, J. R., Bernardo, J. & Remick, D. G. Acute-phase deaths from murine polymicrobial sepsis are characterized by innate immune suppression rather than exhaustion. *The Journal of Immunology* **195**, 3793-3802 (2015).

12 Xiao, H., Siddiqui, J. & Remick, D. G. Mechanisms of mortality in early and late sepsis. *Infection and immunity* **74**, 5227-5235 (2006).

13 Singer, M. The role of mitochondrial dysfunction in sepsis-induced multi-organ failure. *Virulence* **5**, 66-72 (2014).

14 Druml, W., Heinzel, G. & Kleinberger, G. Amino acid kinetics in patients with sepsis. *The American journal of clinical nutrition* **73**, 908-913 (2001).

15 Mecatti, G. C., Messias, M. C. F. & de Oliveira Carvalho, P. Lipidomic profile and candidate biomarkers in septic patients. *Lipids in Health and Disease* **19**, 1-9 (2020).

16 Seymour, C. W. *et al.* Metabolomics in pneumonia and sepsis: an analysis of the GenIMS cohort study. *Intensive care medicine* **39**, 1423-1434 (2013).

17 Quinones, Q. J., Ma, Q., Zhang, Z., Barnes, B. M. & Podgoreanu, M. V. Organ protective mechanisms common to extremes of physiology: a window through hibernation biology. *American Zoologist* **54**, 497-515 (2014).

18 Singer, M., De Santis, V., Vitale, D. & Jeffcoate, W. Multiorgan failure is an adaptive, endocrine-mediated, metabolic response to overwhelming systemic inflammation. *The Lancet* **364**, 545-548 (2004).

19 McCall, C. E. *et al.* Pyruvate dehydrogenase complex stimulation promotes immunometabolic homeostasis and sepsis survival. *JCI insight* **3** (2018).

20 Vary, T. C. Increased pyruvate dehydrogenase kinase activity in response to sepsis. *American Journal of Physiology-Endocrinology and Metabolism* **260**, E669-E674 (1991).

21 Stacpoole, P. W. The pharmacology of dichloroacetate. *Metabolism* **38**, 1124-1144 (1989).

524 22 Zhu, X. *et al.* Stimulating pyruvate dehydrogenase complex reduces itaconate levels and
525 enhances TCA cycle anabolic bioenergetics in acutely inflamed monocytes. *Journal of Leukocyte*
526 *Biology* (2020).
527 23 Kelly, B. & O'neill, L. A. Metabolic reprogramming in macrophages and dendritic cells in innate
528 immunity. *Cell research* **25**, 771-784 (2015).
529 24 Eyenga, P. *et al.* Time course of liver mitochondrial function and intrinsic changes in oxidative
530 phosphorylation in a rat model of sepsis. *Intensive care medicine experimental* **6**, 31 (2018).
531 25 Ilaiwy, A. *et al.* Identification of Metabolic Changes in Ileum, Jejunum, Skeletal Muscle, Liver, and
532 Lung in a Continuous IV Pseudomonas aeruginosa Model of Sepsis Using Nontargeted
533 Metabolomics Analysis. *The American journal of pathology* **189**, 1797-1813 (2019).
534 26 Dahn, M. S., Mitchell, R. A., Lange, M. P., Smith, S. & Jacobs, L. A. Hepatic metabolic response to
535 injury and sepsis. *Surgery* **117**, 520-530 (1995).
536 27 Levy, E., Slusser, R. J. & Ruebner, B. Hepatic changes produced by a single dose of endotoxin in
537 the mouse. Electron microscopy. *The American journal of pathology* **52**, 477 (1968).
538 28 Han, X., Fink, M. P., Uchiyama, T., Yang, R. & Delude, R. L. Increased iNOS activity is essential for
539 hepatic epithelial tight junction dysfunction in endotoxemic mice. *American Journal of*
540 *Physiology-Gastrointestinal and Liver Physiology* **286**, G126-G136 (2004).
541 29 Liu, P. S. *et al.* alpha-ketoglutarate orchestrates macrophage activation through metabolic and
542 epigenetic reprogramming. *Nat Immunol* **18**, 985-994, doi:10.1038/ni.3796 (2017).
543 30 Mills, E. & O'Neill, L. A. Succinate: a metabolic signal in inflammation. *Trends Cell Biol* **24**, 313-
544 320, doi:10.1016/j.tcb.2013.11.008 (2014).
545 31 Mills, E. L. *et al.* Succinate Dehydrogenase Supports Metabolic Repurposing of Mitochondria to
546 Drive Inflammatory Macrophages. *Cell* **167**, 457-470 e413, doi:10.1016/j.cell.2016.08.064
547 (2016).
548 32 Lampropoulou, V. *et al.* Itaconate Links Inhibition of Succinate Dehydrogenase with Macrophage
549 Metabolic Remodeling and Regulation of Inflammation. *Cell Metab* **24**, 158-166,
550 doi:10.1016/j.cmet.2016.06.004 (2016).
551 33 Liao, S. T. *et al.* 4-Octyl itaconate inhibits aerobic glycolysis by targeting GAPDH to exert anti-
552 inflammatory effects. *Nat Commun* **10**, 5091, doi:10.1038/s41467-019-13078-5 (2019).
553 34 Mills, E. L. *et al.* Itaconate is an anti-inflammatory metabolite that activates Nrf2 via alkylation of
554 KEAP1. *Nature* **556**, 113-117, doi:10.1038/nature25986 (2018).
555 35 Daniels, B. P. *et al.* The Nucleotide Sensor ZBP1 and Kinase RIPK3 Induce the Enzyme IRG1 to
556 Promote an Antiviral Metabolic State in Neurons. *Immunity* **50**, 64-76 e64,
557 doi:10.1016/j.immuni.2018.11.017 (2019).
558 36 Indo, H. P. *et al.* Evidence of ROS generation by mitochondria in cells with impaired electron
559 transport chain and mitochondrial DNA damage. *Mitochondrion* **7**, 106-118,
560 doi:10.1016/j.mito.2006.11.026 (2007).
561 37 Soga, T. *et al.* Differential metabolomics reveals ophthalmic acid as an oxidative stress
562 biomarker indicating hepatic glutathione consumption. *J Biol Chem* **281**, 16768-16776,
563 doi:10.1074/jbc.M601876200 (2006).
564 38 Simoes, I. C. M., Fontes, A., Pinton, P., Zischka, H. & Wieckowski, M. R. Mitochondria in non-
565 alcoholic fatty liver disease. *Int J Biochem Cell Biol* **95**, 93-99, doi:10.1016/j.biocel.2017.12.019
566 (2018).
567 39 McCall, C. E. *et al.* Pyruvate dehydrogenase complex stimulation promotes immunometabolic
568 homeostasis and sepsis survival. *JCI Insight* **3**, doi:10.1172/jci.insight.99292 (2018).
569 40 Buck, M. D., Sowell, R. T., Kaech, S. M. & Pearce, E. L. Metabolic Instruction of Immunity. *Cell*
570 **169**, 570-586, doi:10.1016/j.cell.2017.04.004 (2017).

571 41 Singer, M. *et al.* The Third International Consensus Definitions for Sepsis and Septic Shock
572 (Sepsis-3). *JAMA* **315**, 801-810, doi:10.1001/jama.2016.0287 (2016).
573 42 Williams, N. C. & O'Neill, L. A. A role for the Krebs cycle intermediate citrate in metabolic
574 reprogramming in innate immunity and inflammation. *Frontiers in immunology* **9**, 141 (2018).
575 43 Zaslona, Z. & O'Neill, L. A. J. Cytokine-like Roles for Metabolites in Immunity. *Mol Cell*,
576 doi:10.1016/j.molcel.2020.04.002 (2020).
577 44 McGuire, V. A. *et al.* Dimethyl fumarate blocks pro-inflammatory cytokine production via
578 inhibition of TLR induced M1 and K63 ubiquitin chain formation. *Scientific reports* **6**, 31159
579 (2016).
580 45 Della Giustina, A. *et al.* Dimethyl fumarate modulates oxidative stress and inflammation in
581 organs after Sepsis in rats. *Inflammation* **41**, 315-327 (2018).
582 46 Bambouskova, M. *et al.* Electrophilic properties of itaconate and derivatives regulate the
583 IkappaBzeta-ATF3 inflammatory axis. *Nature* **556**, 501-504, doi:10.1038/s41586-018-0052-z
584 (2018).
585 47 Yi, Z. *et al.* IRG1/Itaconate Activates Nrf2 in Hepatocytes to Protect Against Liver Ischemia-
586 Reperfusion Injury. *Hepatology*, doi:10.1002/hep.31147 (2020).
587 48 Zhu, X. *et al.* Stimulating pyruvate dehydrogenase complex reduces itaconate levels and
588 enhances TCA cycle anabolic bioenergetics in acutely inflamed monocytes. *J Leukoc Biol* **107**,
589 467-484, doi:10.1002/JLB.3A1119-236R (2020).
590 49 Giustina, A. D. *et al.* Vitamin B6 reduces oxidative stress in lungs and liver in experimental sepsis.
591 *An Acad Bras Cienc* **91**, e20190434, doi:10.1590/0001-3765201920190434 (2019).
592 50 Chen, J. *et al.* Protective effects of melatonin on sepsis-induced liver injury and dysregulation of
593 gluconeogenesis in rats through activating SIRT1/STAT3 pathway. *Biomed Pharmacother* **117**,
594 109150, doi:10.1016/j.biopha.2019.109150 (2019).
595 51 Langley, R. J. *et al.* An integrated clinico-metabolomic model improves prediction of death in
596 sepsis. *Sci Transl Med* **5**, 195ra195, doi:10.1126/scitranslmed.3005893 (2013).
597 52 Koskinas, J. *et al.* Liver histology in ICU patients dying from sepsis: a clinico-pathological study.
598 *World journal of gastroenterology: WJG* **14**, 1389 (2008).
599 53 Galvan-Pena, S. *et al.* Malonylation of GAPDH is an inflammatory signal in macrophages. *Nat*
600 *Commun* **10**, 338, doi:10.1038/s41467-018-08187-6 (2019).
601 54 van der Veen, J. N. *et al.* (Elsevier, 2017).
602 55 Ling, J., Chaba, T., Zhu, L. F., Jacobs, R. L. & Vance, D. E. Hepatic ratio of phosphatidylcholine to
603 phosphatidylethanolamine predicts survival after partial hepatectomy in mice. *Hepatology* **55**,
604 1094-1102 (2012).
605 56 Li, Z. *et al.* The ratio of phosphatidylcholine to phosphatidylethanolamine influences membrane
606 integrity and steatohepatitis. *Cell metabolism* **3**, 321-331 (2006).
607 57 Listenberger, L. *et al.* Decreasing phosphatidylcholine on the surface of the lipid droplet
608 correlates with altered protein binding and steatosis. *Cells* **7**, 230 (2018).
609 58 Sunshine, H. & Iruela-Arispe, M. L. Membrane lipids and cell signaling. *Current opinion in*
610 *lipidology* **28**, 408 (2017).
611 59 Stacpoole, P. W. The pyruvate dehydrogenase complex as a therapeutic target for age-related
612 diseases. *Aging cell* **11**, 371-377 (2012).
613 60 Min, B. K. *et al.* Pyruvate Dehydrogenase Kinase Is a Metabolic Checkpoint for Polarization of
614 Macrophages to the M1 Phenotype. *Front Immunol* **10**, 944, doi:10.3389/fimmu.2019.00944
615 (2019).
616 61 Huang, B., Wu, P., Bowker-Kinley, M. M. & Harris, R. A. Regulation of pyruvate dehydrogenase
617 kinase expression by peroxisome proliferator-activated receptor-alpha ligands, glucocorticoids,
618 and insulin. *Diabetes* **51**, 276-283, doi:10.2337/diabetes.51.2.276 (2002).

619 62 Hutson, N. J. & Randle, P. J. Enhanced activity of pyruvate dehydrogenase kinase in rat heart
620 mitochondria in alloxan-diabetes or starvation. *FEBS Lett* **92**, 73-76, doi:10.1016/0014-
621 5793(78)80724-8 (1978).
622 63 Baxter, M. A. & Coore, H. G. The mode of regulation of pyruvate dehydrogenase of lactating rat
623 mammary gland. Effects of starvation and insulin. *Biochem J* **174**, 553-561,
624 doi:10.1042/bj1740553 (1978).
625 64 Fuller, S. J. & Randle, P. J. Reversible phosphorylation of pyruvate dehydrogenase in rat skeletal-
626 muscle mitochondria. Effects of starvation and diabetes. *Biochem J* **219**, 635-646,
627 doi:10.1042/bj2190635 (1984).
628 65 Denyer, G. S., Kerbey, A. L. & Randle, P. J. Kinase activator protein mediates longer-term effects
629 of starvation on activity of pyruvate dehydrogenase kinase in rat liver mitochondria. *Biochem J*
630 **239**, 347-354, doi:10.1042/bj2390347 (1986).
631 66 Wu, P. *et al.* Starvation increases the amount of pyruvate dehydrogenase kinase in several
632 mammalian tissues. *Arch Biochem Biophys* **381**, 1-7, doi:10.1006/abbi.2000.1946 (2000).
633 67 Klyuyeva, A., Tuganova, A., Kedishvili, N. & Popov, K. M. Tissue-specific kinase expression and
634 activity regulate flux through the pyruvate dehydrogenase complex. *J Biol Chem* **294**, 838-851,
635 doi:10.1074/jbc.RA118.006433 (2019).
636 68 Bao, H., Kasten, S. A., Yan, X. & Roche, T. E. Pyruvate dehydrogenase kinase isoform 2 activity
637 limited and further inhibited by slowing down the rate of dissociation of ADP. *Biochemistry* **43**,
638 13432-13441, doi:10.1021/bi049488x (2004).
639 69 Pratt, M. L. & Roche, T. E. Mechanism of pyruvate inhibition of kidney pyruvate dehydrogenasea
640 kinase and synergistic inhibition by pyruvate and ADP. *J Biol Chem* **254**, 7191-7196 (1979).
641 70 Vachharajani, V. T. *et al.* SIRT1 inhibition during the hypoinflammatory phenotype of sepsis
642 enhances immunity and improves outcome. *J Leukoc Biol* **96**, 785-796,
643 doi:10.1189/jlb.3MA0114-034RR (2014).
644 71 Chen, Z., Fitzgerald, R. L., Averna, M. R. & Schonfeld, G. A targeted apolipoprotein B-38.9-
645 producing mutation causes fatty livers in mice due to the reduced ability of apolipoprotein B-
646 38.9 to transport triglycerides. *J Biol Chem* **275**, 32807-32815, doi:10.1074/jbc.M004913200
647 (2000).
648 72 Dobin, A. *et al.* STAR: ultrafast universal RNA-seq aligner. *Bioinformatics* **29**, 15-21,
649 doi:10.1093/bioinformatics/bts635 (2013).
650 73 Liao, Y., Smyth, G. K. & Shi, W. featureCounts: an efficient general purpose program for
651 assigning sequence reads to genomic features. *Bioinformatics* **30**, 923-930,
652 doi:10.1093/bioinformatics/btt656 (2014).
653 74 Quinn, M. A., Xu, X., Ronfani, M. & Cidlowski, J. A. Estrogen Deficiency Promotes Hepatic
654 Steatosis via a Glucocorticoid Receptor-Dependent Mechanism in Mice. *Cell Rep* **22**, 2690-2701,
655 doi:10.1016/j.celrep.2018.02.041 (2018).

656

657

658

659

660 **Figure Legends**

661 **Figure 1: Sepsis Impairs hepatic mitochondrial metabolism.** (A) Top 5 canonical
662 pathways subject to transcriptional alterations in the liver identified by Ingenuity Pathway
663 Analysis of RNA-seq of sham versus CLP mice (n = 4 mice per group). Blue represents
664 a negative z-score and orange represents a positive z-score. Shading indicates intensity
665 of pathway activation/inhibition. (B) GSEA of the oxidative phosphorylation pathway
666 (GO:0006119) indicating a negative normalized enrichment score (NES = -0.853). (C)
667 GSEA of the TCA cycle pathway (GO:0006099) indicating a negative enrichment score
668 (NES = -1.1956). (D) Schematic representation of hepatic TCA cycle metabolites altered
669 during chronic sepsis. Red denotes a metabolite increased in response to sepsis; green
670 indicates a metabolite decreased in response to sepsis; black indicates a metabolite un-
671 changed in response to sepsis; grey indicates a metabolite not measured in our metabo-
672 lomic screening. (E-J) Relative metabolite levels measured by Ultrahigh Performance Liq-
673 uid Chromatography-Tandem Mass Spectroscopy (UPLC-MS/MS) from livers of sham
674 and CLP mice 30 hours post-surgery (n = 5 sham; 8 CLP). (K) rlog transformed counts
675 from RNA-seq of sham and CLP mice 30 hours post-surgery. (L) Relative itaconate levels
676 in livers of sham and CLP mice measured by UPLC-MS/MS (n = 5 sham; 8 CLP). * de-
677 notes $p<0.05$.

678

679 **Figure 2: Impaired hepatic redox balance in septic mice.** (A) GSEA of the ROS met-
680 abolic pathway (GO:0072593) from RNA-seq from livers comparing sham to CLP showing
681 a positive enrichment score (NES = 1.117) (n = 4 mice per group). (B-F) Relative metab-
682 olite levels of metabolites involved in redox balance measured by UPLC-MS/MS (n = 5

683 sham; 8 CLP). (G) Relative levels of ophthalmate involved in redox balance measured by
684 UPLC-MS/MS. * denotes p<0.05, ** p<0.01, **** p<0.0001.

685

686 **Figure 3: Sepsis promotes hepatic steatosis.** (A) Top 5 induced and repressed physi-
687 ological pathways in the liver of sham versus CLP mice identified by IPA of RNA-seq. (B)
688 GSEA of the fatty acid metabolic pathway (GO:0019395) from RNA-seq from livers com-
689 paring sham to CLP showing a negative enrichment score (NES = -1.018) (n = 4 mice per
690 group). (C) IPA of top 5 metabolic pathways significantly altered in the liver in response
691 to sepsis identified by global metabolomic screening. (D) Heatmap representation of log2
692 fold change of different lipid species in sham and CLP mice measured by UPLC-MS/MS.
693 (E) Quantification of lipids by UPLC-MS/MS in hepatocytes isolated from sham and CLP
694 mice 30 hours post-surgery (n = 5 sham; n = 8 CLP). * denotes p<0.05, ** p<0.01, ***
695 p<0.001.

696

697 **Figure 4: Sepsis reprograms the hepatic lipidome.** (A) Volcano plot of significantly
698 altered lipids from sham and CLP hepatocytes measured by UPLC-MS/MS (n = 5 sham;
699 n = 8 CLP). (B) Pie chart of lipid compositions from sham and CLP mice. (C) Quantifica-
700 tion of lipids by UPLC-MS/MS in hepatocytes isolated from sham and CLP mice 30 hours
701 post-surgery (n = 5 sham; n = 8 CLP). ** denotes p<0.01, *** p<0.001, **** p<0.0001.

702

703 **Figure 5: PDK inhibition restores hepatic metabolism in septic mice.** (A) Venn dia-
704 gram of differentially expressed genes (DEGs) assessed by RNA-seq in CLP versus

705 sham compared to CLP+DCA versus sham 30 hours post-surgery (left). Heatmap of av-
706 erage log2 fold change of DEGs in sham, CLP and CLP+DCA (right) (n = 4 mice per
707 group). (B) Heatmap depiction of z-scores of top canonical pathways identified by IPA in
708 CLP versus sham and CLP+DCA versus sham. (C) Heatmap depiction of average log2
709 fold change in metabolite levels involved in redox balance in sham, CLP and CLP+DCA
710 24 hours post-surgery measured by UPLC-MS/MS (n = 5 sham; n = 8 CLP and
711 CLP+DCA). (D) Heatmap depiction of average log2 fold change in metabolite levels in-
712 volved in TCA cycle in sham, CLP and CLP+DCA 30 hours post-surgery measured by
713 UPLC-MS/MS (n = 5 sham; n = 8 CLP and CLP+DCA). (E) Heatmap depiction of average
714 log2 fold change in MAG, DAG and TAG levels in sham, CLP and CLP+DCA 30 hours
715 post-surgery measured by UPLC-MS/MS (n = 5 sham; n = 8 CLP and CLP+DCA). (F)
716 Heatmap depiction of average log2 fold change in phospholipids in sham, CLP and
717 CLP+DCA 30 hours post-surgery measured by UPLC-MS/MS (n = 5 sham; n = 8 CLP
718 and CLP+DCA.

719

720

721

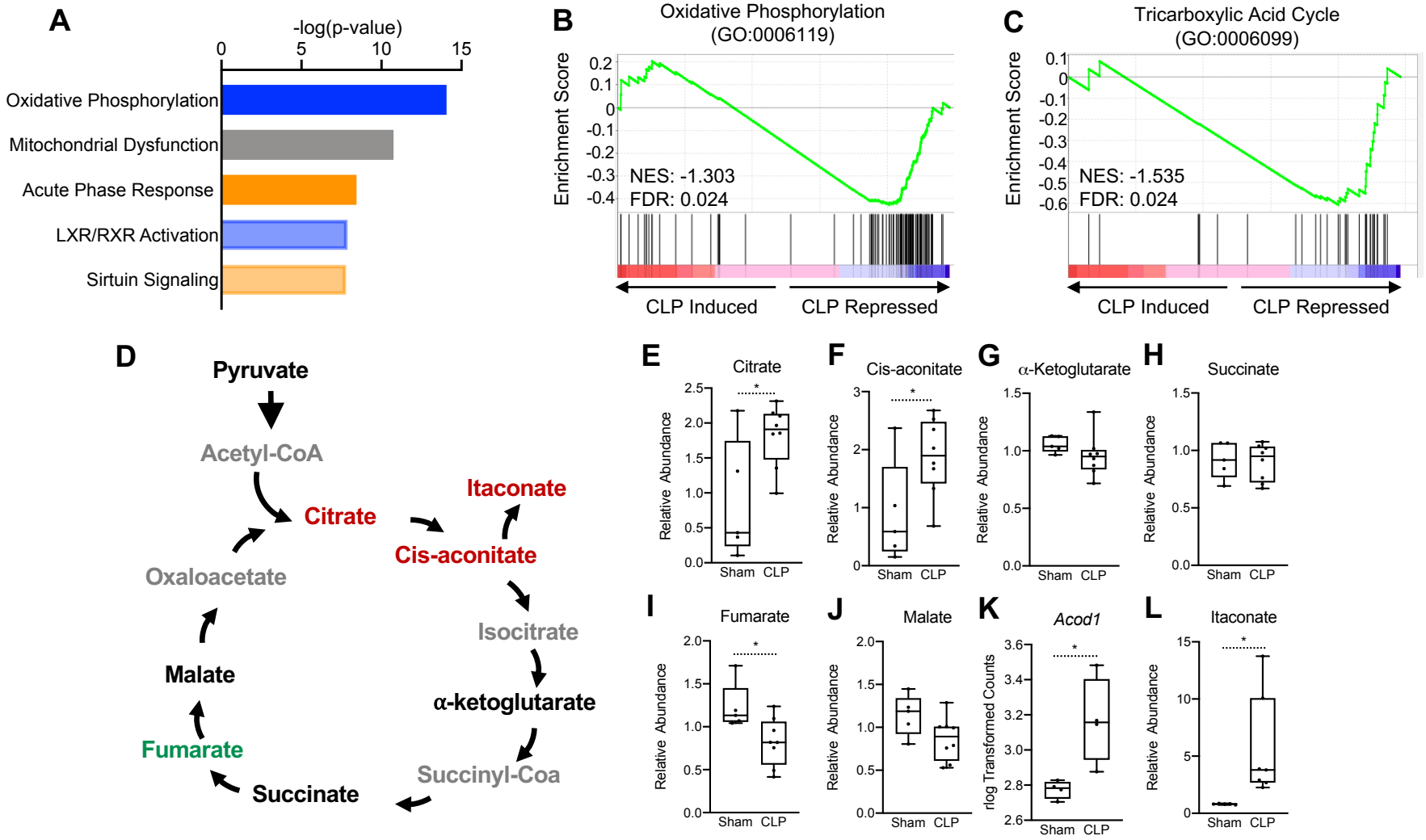

Figure 1: Sepsis Impairs Hepatic Mitochondrial Metabolism

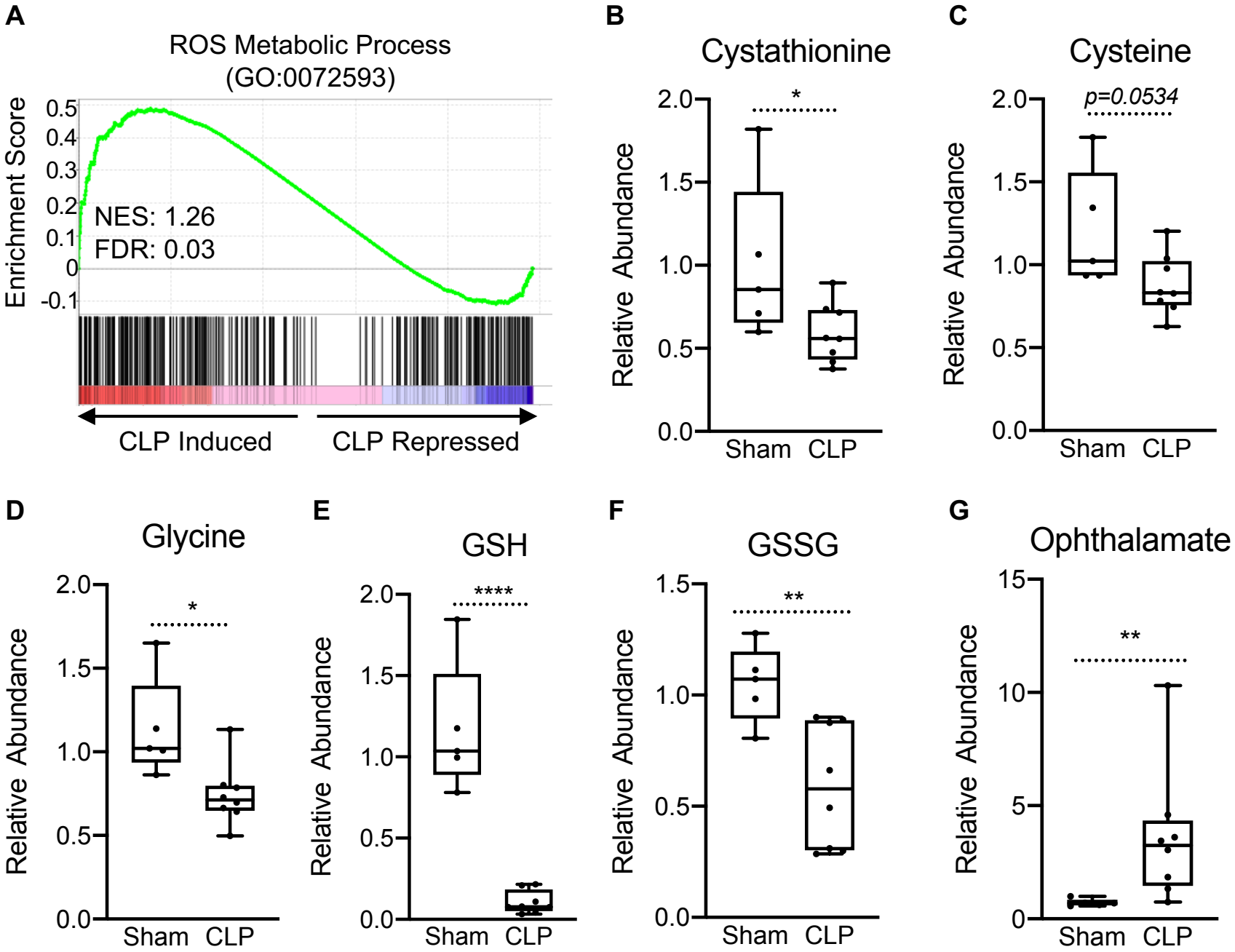

Figure 2: Impaired Hepatic Redox Balance in Septic Mice

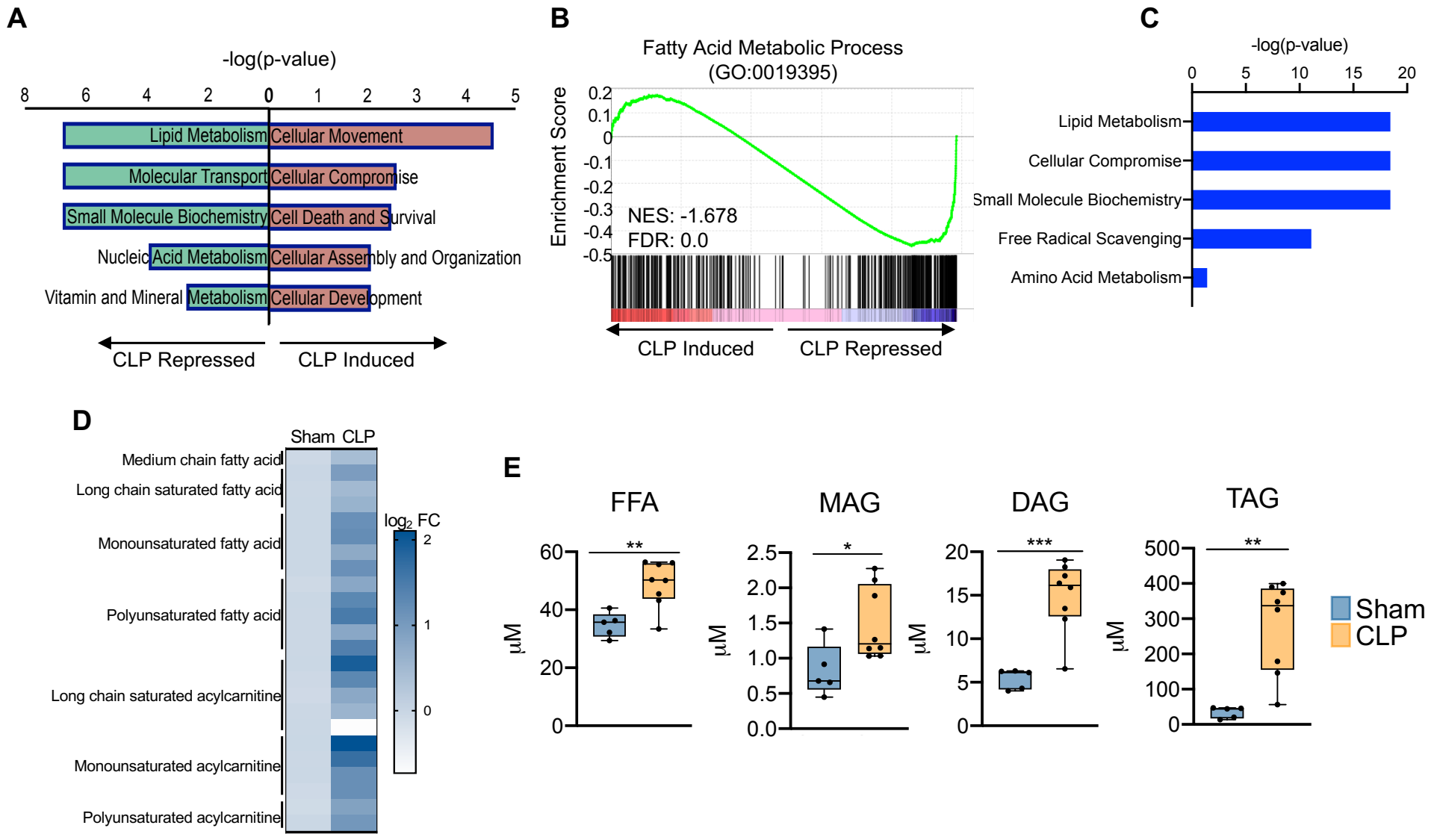

Figure 3: Sepsis promotes hepatic steatosis

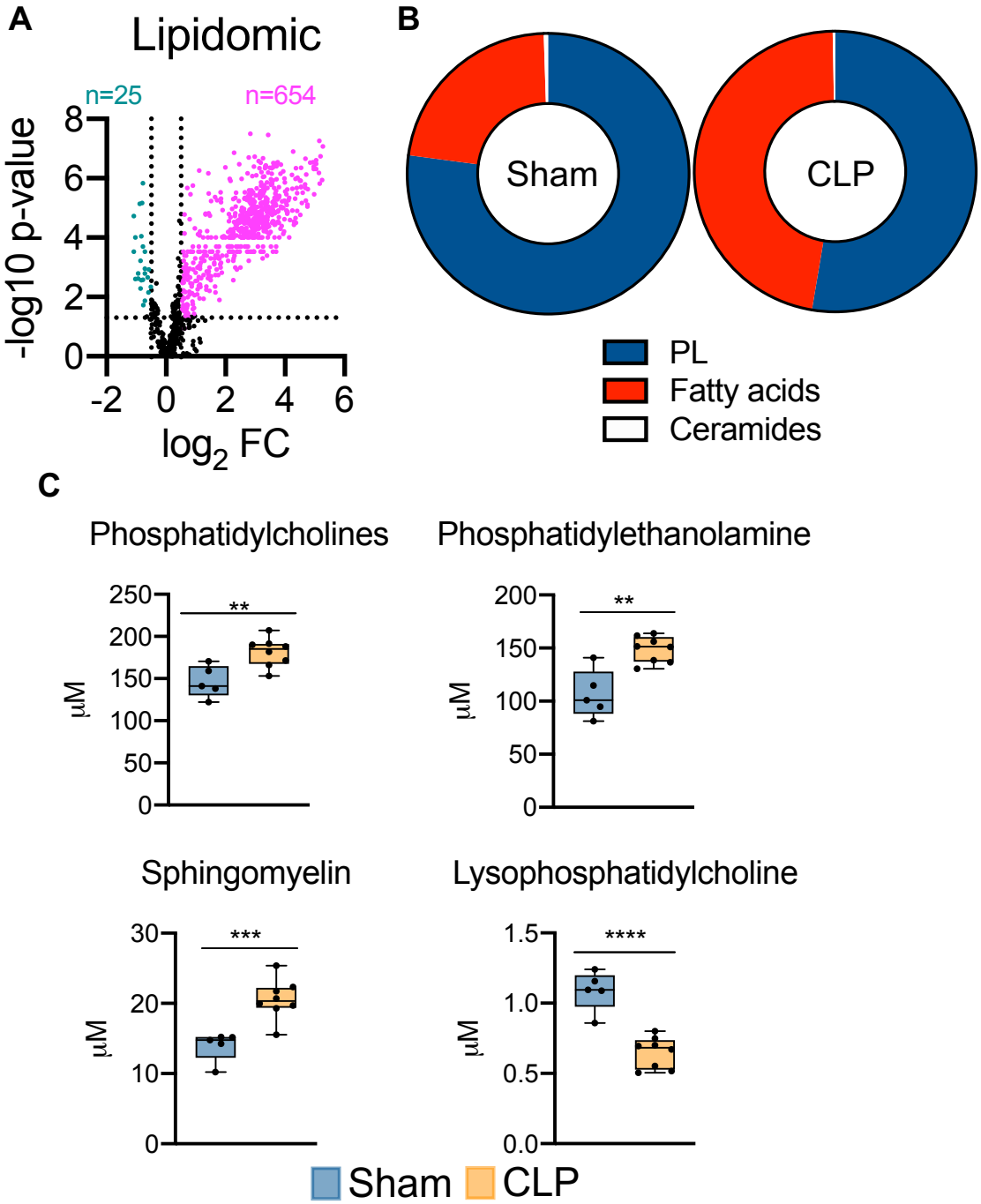

Figure 4: Sepsis reprograms the hepatic lipidome

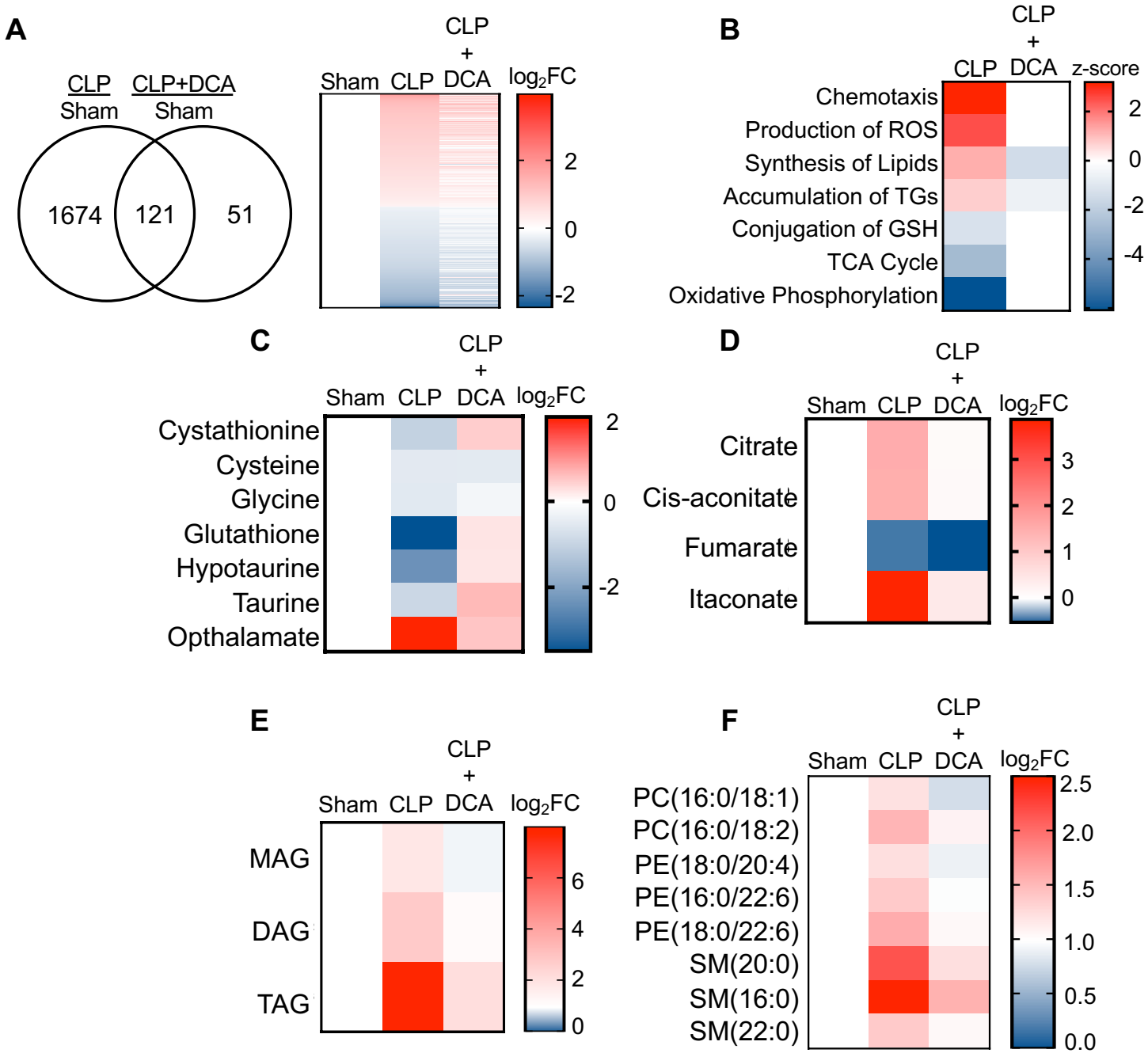

Figure 5: DCA reverses transcriptional and metabolic changes elicited by sepsis in the liver

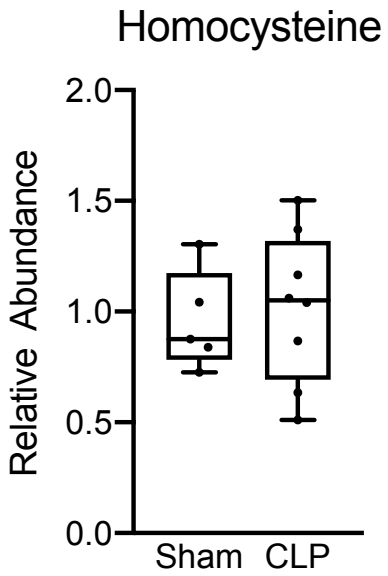

Supplemental figure 1: Hepatic homocysteine levels in sham and CLP mice. Ultrahigh Performance Liquid Chromatography-Tandem Mass Spectroscopy measurement of homocysteine from isolated hepatocytes 30 hours post-surgery. n=5 sham, n=8 CLP.

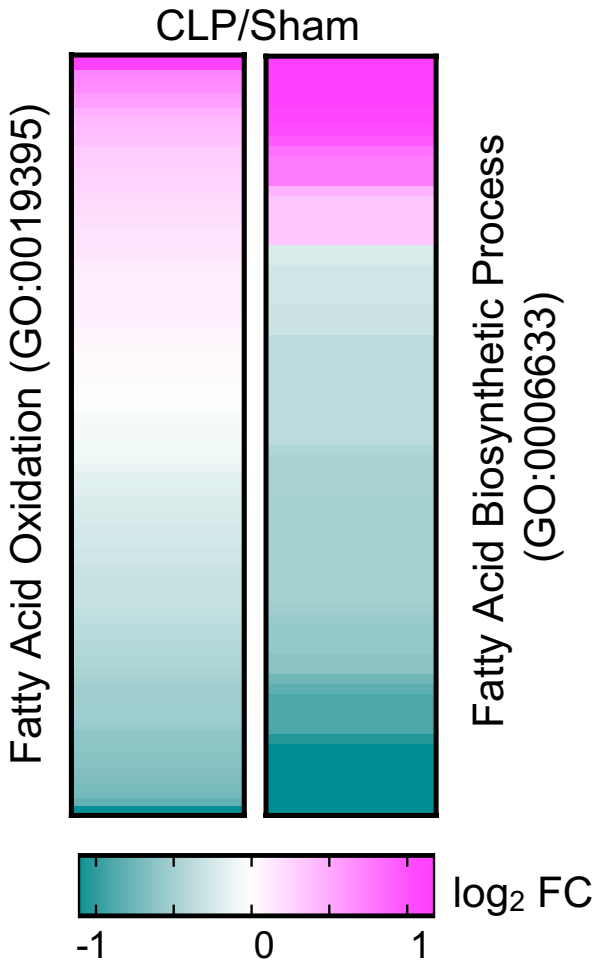

Supplemental figure 2: Fatty acid oxidation and biosynthetic pathways in septic livers. Heatmap representation of average log2 fold change of genes involved in fatty acid oxidation (GO:0019395) and fatty acid biosynthetic process (GO:0006633) in CLP versus sham operated mice (n = 5 sham; n = 8 CLP).

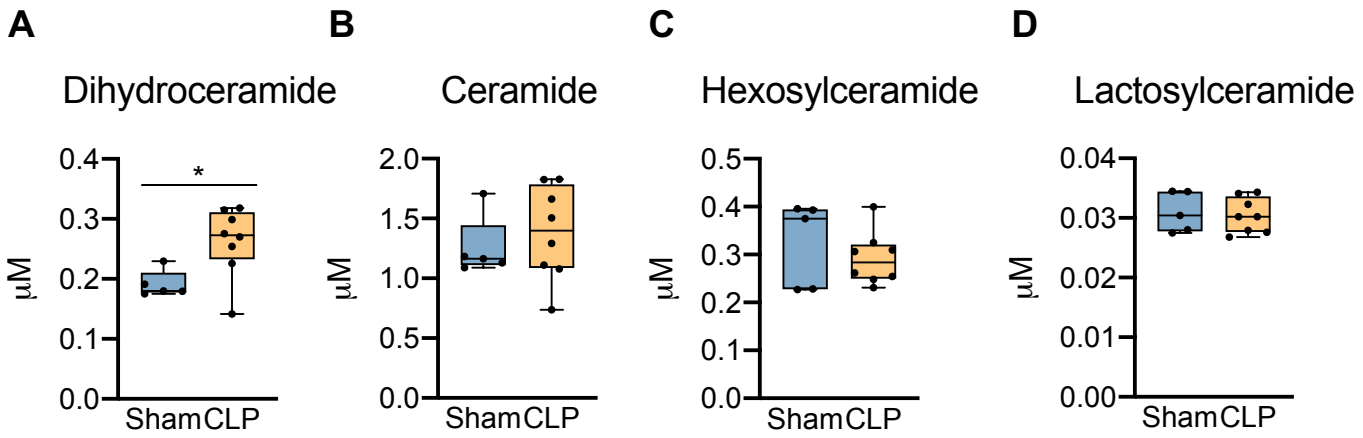

Supplemental figure 3: Hepatic ceramide levels in sham and CLP mice. Ultrahigh Performance Liquid Chromatography-Tandem Mass Spectroscopy measurement of **(A)** dihydroceramide, **(B)** ceramide, **(C)** hexosylceramide and **(D)** lactosylceramide from isolated hepatocytes 30 hours post-surgery. n=5 sham, n=8 CLP. * denotes $p<0.05$ determined by Student's T-test.

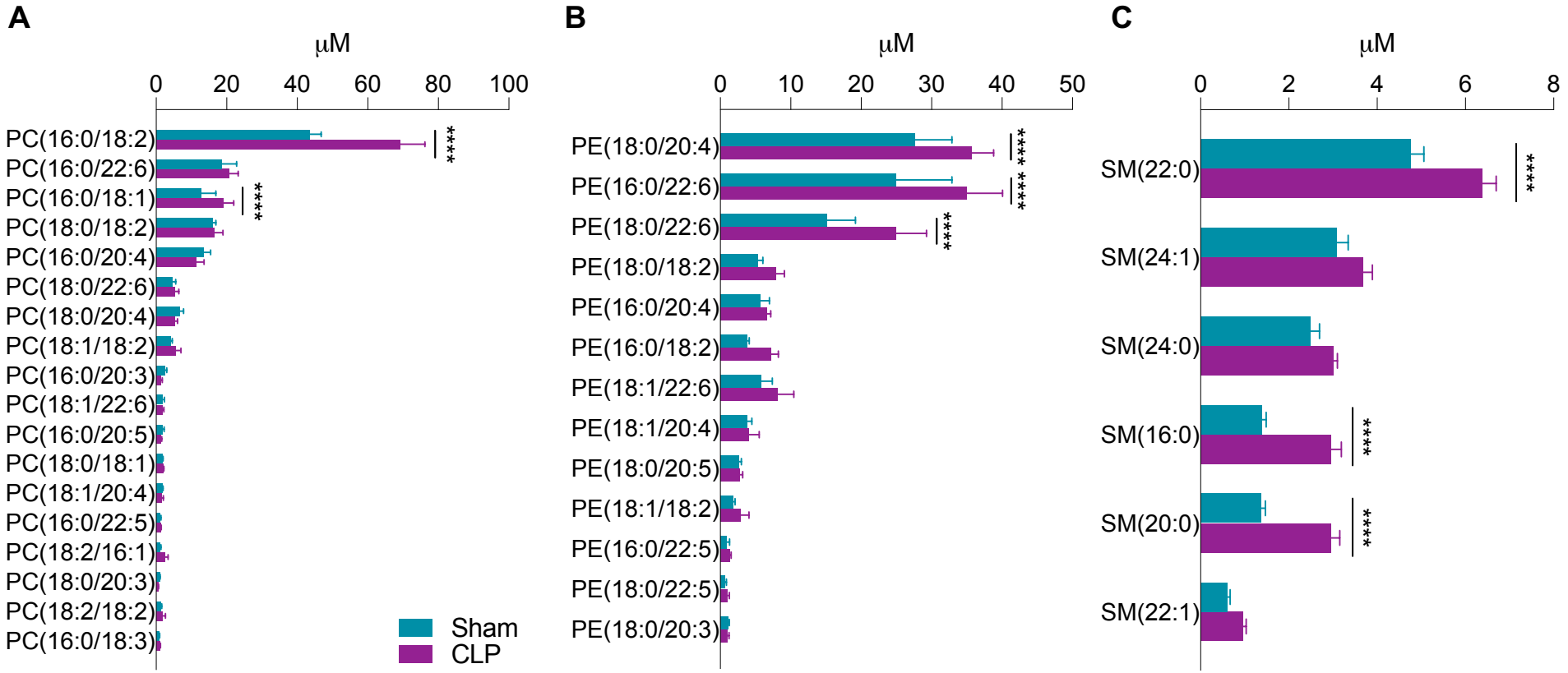

Supplemental figure 4: Phosphatidylcholine, phosphatidylethanolamine, and sphingomyelin quantifications. Ultrahigh Performance Liquid Chromatography-Tandem Mass Spectroscopy measurement of **(A)** phosphatidylcholine species, **(B)** phosphatidylethanolamine species and **(C)** sphingomyelin species from isolated hepatocytes 30 hours post-surgery. n=5 sham, n=8 CLP. **** denotes $p<0.0001$ determined by two-way ANOVA followed by multiple comparisons test.

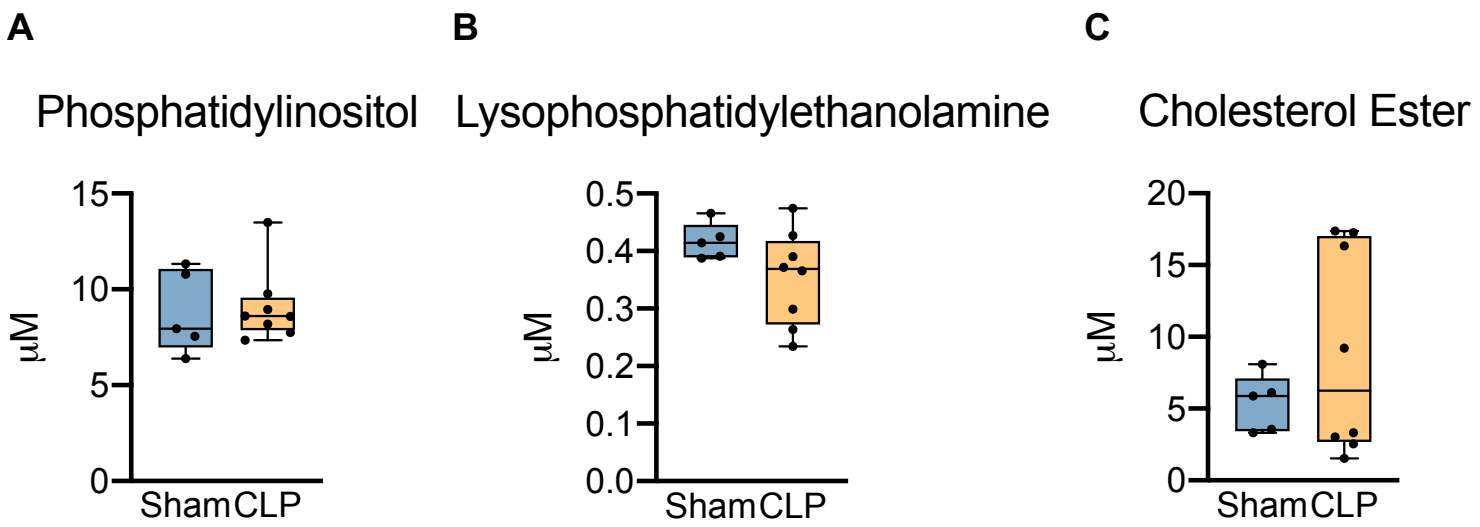

Supplemental figure 5: PI, LPE and CE levels in septic livers. Ultrahigh Performance Liquid Chromatography-Tandem Mass Spectroscopy measurement of **(A)** phosphatidylinositol, **(B)** lysophosphatidylethanolamine species and **(C)** cholesterol ester from isolated hepatocytes 30 hours post-surgery. n=5 sham, n=8 CLP. **** denotes $p<0.0001$ determined by two-way ANOVA followed by multiple comparisons test.